

High-Intensity Focused Ultrasound (HIFU) Multiple Lesion Imaging: Comparison of Detection Algorithms for Real-Time Treatment Control

Ralf Seip*, Jahangir Tavakkoli, Roy F. Carlson, Adam Wunderlich, Narendra T. Sanghvi
Focus Surgery, Inc. Indianapolis, IN 46226

Kris A. Dines

XDATA Corporation, Indianapolis, IN 46220

Thomas A. Gardner

Dept. of Urology, Indiana Univ. School of Medicine, Indianapolis, IN 46202

Abstract – Imaging of HIFU-induced lesions provides non-invasive, real-time treatment monitoring and control. This work presents results obtained with HIFU-induced lesion detection algorithms specifically designed for multiple lesion detection. Algorithms sensitive to *relative* tissue changes during HIFU - measuring signal energy, tissue displacement, entropy, and tissue attenuation are compared for their ability to detect the creation of multiple and adjacent HIFU lesions. *In vivo* (N=4) canine prostate backscattered RF data was acquired with a custom Sonablate®500 HIFU device during 7 treatments. A total of 815 sites were treated, forming the algorithm evaluation dataset. It was found that the algorithm based on signal energy performed best, detecting 82% of all HIFU lesions created, while showing false-alarm rates below 5%. All methods are completely non-invasive, and make use of tissue reference/normalization information obtained before, during, and after the HIFU treatment. Algorithm specifics, data acquisition methodologies, *in vivo* experimental results, and algorithm comparison results are shown.

I. INTRODUCTION

HIFU exposures create lesions of therapeutic benefit in tissue through rapid temperature elevation in the focal region. Lesion detection enables users to monitor, control, and assess HIFU treatments non-invasively in real-time. Lesion detection techniques utilizing diagnostic ultrasound are based on the hypothesis that the backscattered RF signal acquired from the focal zone of the HIFU transducer during treatment contains information which can be extracted using signal processing techniques to monitor and image (directly or indirectly) the HIFU-induced lesions. Previous work in this area has shown promising results [1-6]. However, that work focused

mainly on detecting single lesions, while we report on the clinical necessity to detect the consecutive placement of multiple HIFU elementary lesions that are required to treat large tissue volumes [7-9]. Conventional B-mode ultrasound imaging does not provide reliable HIFU lesion imaging. Clearly, a different, quantitative, robust, and automated approach for multiple lesion visualization and/or detection is required. This paper evaluates four different lesion detection algorithm candidates that are sensitive to different physical tissue parameters, and compares their performance for providing quantitative lesioning information for HIFU treatment monitoring and eventual automated treatment control.

II. MATERIALS AND METHODS

Data Acquisition Methodology

To support the development and evaluation of the multiple lesion detection algorithm candidates, *in vivo* RF backscattered data was acquired from 4 canine prostates during 7 HIFU treatments with the imaging transducer of a modified Sonablate®500 HIFU system and stored for processing. These 1D signals always image the region containing the focal zone of the therapy transducer, as shown in Figure 1.

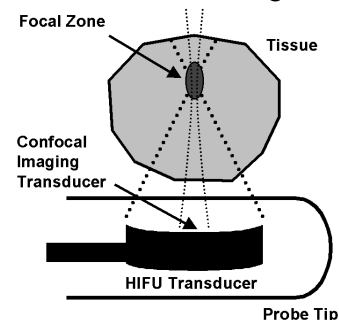


Figure 1: Confocal arrangement of imaging transducer with the therapy transducer.

Data was acquired pre-treatment ("T=-∞"), pre-lesion (T=0s), during HIFU lesioning (0<T≤3s), and after lesion creation (3<T<9s) for each treatment site, as indicated by the solid vertical lines in Figure 2. A single elementary lesion is created at each treatment site (815 total for the 7 HIFU treatments). To acquire interference-free data during the HIFU "ON" time, HIFU delivery is briefly interrupted for 70ms every 500ms. During the treatment, the lesion detection algorithm also processes this data in real-time to generate a lesion overlay that is displayed on the treatment screen (Figure 4), and updated during the times indicated by the dashed vertical lines shown in Figure 2.

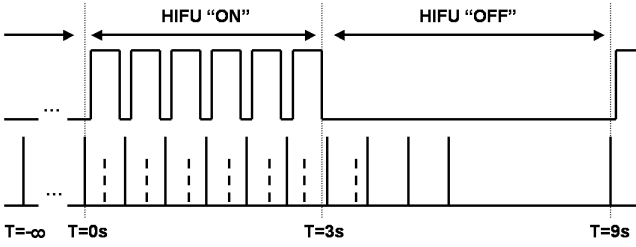


Figure 2: RF data acquisition methodology.

A total of 4 different multiple-lesion detection algorithm candidates were evaluated for their ability to detect the creation of the HIFU-induced lesions. These algorithms compute the relative changes in backscattered *signal energy* (due to tissue structure changes, cavitation, or vapor bubbles), *tissue displacement* (due to thermal expansion or the thermal dependence of the speed of sound in the medium), *signal entropy* (due to tissue structure changes), and *attenuation* (due to temperature-dependent attenuation [10]) between the pre-lesion reference signal acquired at T=0s and subsequently acquired signals during the HIFU exposure.

In all approaches, $p(n, T)$ is the parameter indicative of the lesion that is displayed as a color overlay during the HIFU treatment, n is the index into the echo data (in depth, or "fast time"), and T is the treatment time index ("slow time"). $Echo(n, T)$ refers to the RF backscattered data acquired at time T (every 500ms) for the current lesion site, and wf is a specified data windowing function. For analysis and display, $p(n, T)$ is computed for pre-focal, focal, and post-focal regions to localize the lesion in depth n . Algorithm implementation specifics are shown in Table 1, and were chosen to optimize the detection ability of each approach.

Implementation Parameters

	Signal Energy	Tissue Displacement	Signal Entropy	Attenuation Change
Data Length	1.92 mm (~5λ)	3.0 mm (8λ)	1.92 mm (~5λ)	4.5 mm (12λ)
Data Overlap	0.96 mm (~2.5λ)	1.5 mm (4λ)	0.96 mm (~2.5λ)	2.25 mm (6λ)
Window Function	Tukey (15% taper)	None	Tukey (15% taper)	Blackman
Reference	T ₀	T ₀	T ₀	T ₀
Pre-Processing	Mean Removal	Mean Removal Envelope Detection	Mean Removal Envelope Detection	Mean Removal
Post-Processing	4-point Smoothing Filter	3-point Median Filter Low SNR estimate removal Cumulative Displacement	4-point Smoothing Filter	4-point Smoothing Filter

Table 1: Lesion detection algorithm implementation specifics.

The mathematical description of the lesion detection algorithm candidates is given below.

- *Signal Energy*

$$p(n, T) = \frac{E_{signal} - E_{reference}}{E_{reference}}$$

$$E_{signal} = \sum_{window(n)} [wf \cdot echo(n, T)]^2$$

$$E_{reference} = \sum_{window(n)} [wf \cdot echo(n, T_0)]^2$$

- *Tissue Displacement*

$$p(n, T) = displacement[echo(n, T - \Delta T), echo(n, T)]$$

- *Signal Entropy*

$$p(n, T) = H_{signal} - H_{reference}$$

$$H_{signal} = \sum_{k=0}^{N-1} p_{k(signal)} \cdot \log_2(p_{k(signal)})$$

$$H_{reference} = \sum_{k=0}^{N-1} p_{k(reference)} \cdot \log_2(p_{k(reference)})$$

where p_k indicates the probability that the symbol k is present in the echo signal, and $N = 2^b - 1$, where $b=6$ is the number of quantization bits.

- Attenuation Change

$p(n, T) = \text{value at } f_{\max} \text{ of best line fit to } \Delta S(f)$

$$\Delta S(f) = S(f)_{\text{signal}} - S(f)_{\text{reference}} \\ \sim -2A(f)d, \text{ in [dB]}$$

$$S(f)_{\text{signal}} = 20 \log_{10}[| \text{fft}(wf \cdot \text{echo}(n, T)) |]$$

$$S(f)_{\text{reference}} = 20 \log_{10}[| \text{fft}(wf \cdot \text{echo}(n, T_0)) |]$$

III. RESULTS

All detection algorithms were evaluated against the canine *in vivo* data set collected during the HIFU treatments. The parameter $p(n, T)$ was computed for all 815 sites using the 4 candidate algorithms. Algorithm performance was evaluated by determining whether or not $p(n, T)$ highlighted the created lesion. Figure 3 shows an example of $p(n, T)$ computed off-line with the attenuation change algorithm for 20 individual treatment sites as a function of treatment time T (horizontal axis, in [s]), and depth n (vertical axis, in [mm]). Clearly, lesions can be seen forming at all sites except 8, 17, and 18. In this example, the algorithm correctly detected 17 out of 20 lesions. For algorithm performance comparison purposes, it was assumed that each HIFU shot generated a HIFU lesion at each treatment site.

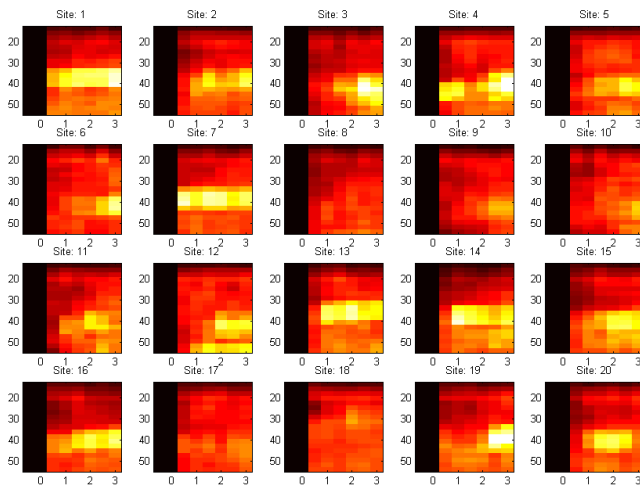


Figure 3: Lesion detection output $p(n, T)$ example computed for 20 lesion sites for algorithm evaluation.

The performance of the lesion detection algorithms is summarized in Table 2. It shows that the simple,

signal energy-based detection algorithm (normalized and referenced to the pre-lesion dataline at T_0) performs the best at detecting the multiple HIFU-induced lesions.

	Lesions Detected	False Alarm
Signal Energy	82%	4%
Tissue Displacement	76%	10%
Signal Entropy	49%	14%
Attenuation Change	71%	2%

Table 2: Lesion detection algorithm performance.

This algorithm was implemented for its clinical evaluation in a custom Sonablate[®] 500 HIFU system. It enables the user to monitor the evolution and computed extent of the lesions in real-time during a HIFU treatment. Relatively good agreement exists between the detected lesion size and shape to the actual lesion as verified histologically. The computed lesion overlay can be seen on the top linear image of the treatment screen of the Sonablate (Figure 4).

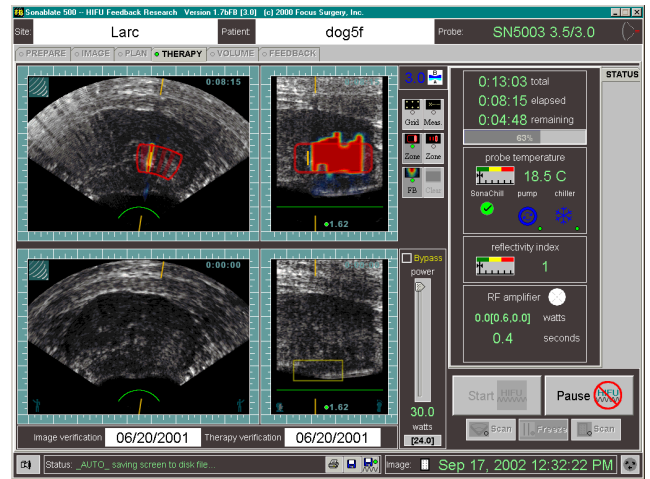


Figure 4: Real-time implementation and example of results of signal energy lesion detection algorithm and overlay in commercially available Sonablate[®] 500 HIFU system.

IV. DISCUSSION AND CONCLUSIONS

The results show that it is possible to implement a real-time lesion detection algorithm based entirely on 1D backscattered RF data that can produce clinically useful information for HIFU treatments. Overlaying treatment feedback data on conventional B-mode images was also found to be an effective and intuitive

way of displaying such information to the user. Out of all of the multiple lesion detection algorithm candidates examined, the signal energy-based algorithm (referenced to the pre-lesion echo acquired at T_0) performed best, detecting 82% of HIFU-induced lesions.

The *in vivo* results also showed that the pre-treatment (" $T=-\infty$ ") echo is not suitable for algorithm calibration/normalization. It decorrelates with respect to the pre-lesion echoes within several minutes into the treatment due to motion and cumulative HIFU-induced changes to the treated tissue. Thus far, the pre-lesion ($T=T_0$) echo is essential in the detection process, providing a baseline from which the relative estimates of tissue change due to HIFU are computed.

Even though these results are encouraging, it is believed that none of the algorithms developed thus far *directly* image the lesion itself, but rather image *indirect* indications of the lesioning process. Such indirect indications include the detection of cavitation bubbles and vapor bubbles. This observation partially explains the good results obtained with the signal energy algorithm: bubbles easily change the amount of backscattered energy, the parameter to which the signal energy algorithm is sensitive to. The poor results obtained with the signal entropy method suggest that HIFU treatments rapidly change the tissue structure, even over short (<500ms) timescales, making it difficult to detect the lesion formation as clearly shown in Figure 3.

The results have provided a guide to determine where current and future efforts are focused. Work is underway in the following areas:

- Evaluating alternate (non-linear, pattern matching, etc.) multiple lesion detection algorithms.
- Distinguishing between direct and indirect lesion imaging by performing overpressure experiments to suppress the formation of cavitation/vapor bubbles.
- Examining pre-focal activity to determine if a purely thermal effect (i.e. direct lesion indicator) can be isolated for HIFU lesion imaging that would not be affected by bubble activity.

ACKNOWLEDGEMENTS

The authors would like to thank the staff of the Indiana University School of Medicine at the Large

Animal Research Center (LARC) for their help with the *in vivo* canine experiments. This work was funded by NIH SBIR Grant 2 R44 CA83244-02.

REFERENCES

- [1] Wear, K., Wagner, R., Insana, M., Hall, T., "Application of Autoregressive Spectral Analysis to Cepstral Estimation of Mean Scatterer Spacing" in *IEEE Transactions on Ultrasonics, Ferroelectrics, and Frequency Control*, Vol. 40, pp. 50-58, 1993.
- [2] Greenleaf, J.F., *Tissue Characterization with Ultrasound*, Boca Raton: CRC Press, 1986.
- [3] Ribault, M., Chapelon, J.Y., Cathignol, D., and Gelet, A., "Differential Attenuation Imaging for the Characterization of High Intensity Focused Ultrasound Lesions" in *Ultrasound Imaging*, Vol. 20, pp. 160-177, 1998.
- [4] Seip, R., Feedback for Ultrasound Thermotherapy, Ph.D. Dissertation, The University of Michigan, 1996.
- [5] Fry, F.J., Sanghvi, N.T., Morris, R.F., Smithson, S., Atkinson, L., Dines, K., Franklin, T., and Hastings, J., "A Focused Ultrasound System for Tissue Volume Ablation in Deep Seated Brain Sites" in *Ultrasonics Symposium Proceedings*, Vol. 1, 1001-1004, 1986.
- [6] Bevan, P.D., and Sherar, M.D., "B-Scan Ultrasound Imaging of Thermal Coagulation in Bovine Liver: Frequency Shift Attenuation Mapping" in *Ultrasound in Medicine and Biology*, Vol. 27, No. 6, pp. 809-817, 2001.
- [7] Muschter, R., Bohlen, D., Thuroff, S., Ebert, T., and Madersbacher, S., "High Intensity Focused Ultrasound in Urology: Consensus Report", *High Energy Shock Waves in Medicine: Clinical Application in Urology, Gastroenterology, and Orthopedics*, Georg Thieme Verlag, Stuttgart - New York, 1997, pp. 140-146.
- [8] Sanghvi, N.T., Fry, F.J., Bihrl, R., Foster, R.S., Phillips, M.H., Syrus, J., Zaitsev, A.V., and Hennige, C.W., "Non-Invasive Surgery of Prostate Tissue by High Intensity Focused Ultrasound" in *IEEE Transactions on Ultrasonics, Ferroelectrics, and Frequency Control*, Vol. 43, pp. 1099-1110, 1996.
- [9] Madersbacher, S. and Marberger, M., "High-Intensity Focused Ultrasound in Urology," *J. of Endourology*, Vol. 9, No. 1, pp. 5-15, 1996.
- [10] Damianou, C.A., Sanghvi, N.T., Fry, F.J., and Maass-Moreno, R., "Ultrasonic Attenuation and Absorption Dependence on Temperature and Thermal Dose in Dog Soft Tissue," in *J. Acoust. Soc. Am.*, July 1997.

* rseip@focus-surgery.com